WATER RESOURCES RESEARCH, VOL. 49, 5395–5410, doi:10.1002/wrcr.20356, 2013

Aquifer heterogeneity characterization with oscillatory pumping: Sensitivity analysis and imaging potential

M. Cardiff,[1,2] T. Bakhos,[3] P. K. Kitanidis,[3] and W. Barrash[1]

Received 11 April 2012; revised 31 May 2013; accepted 4 June 2013; published 5 September 2013.

[1] Periodic pumping tests, in which a fluid is extracted during half a period, then reinjected, have been used historically to estimate effective aquifer properties. In this work, we suggest a modified approach to periodic pumping test analysis in which one uses several periodic pumping signals of different frequencies as stimulation, and responses are analyzed through inverse modeling using a "steady-periodic" model formulation. We refer to this strategy as multifrequency oscillatory hydraulic imaging. Oscillating pumping tests have several advantages that have been noted, including no net water extraction during testing and robust signal measurement through signal processing. Through numerical experiments, we demonstrate additional distinct advantages that multifrequency stimulations have, including: (1) drastically reduced computational cost through use of a steady-periodic numerical model and (2) full utilization of the aquifer heterogeneity information provided by responses at different frequencies. We first perform fully transient numerical modeling for heterogeneous aquifers and show that equivalent results are obtained using a faster steady-periodic heterogeneous numerical model of the wave phasor. The sensitivities of observed signal response to aquifer heterogeneities are derived using an adjoint state-based approach, which shows that different frequency stimulations provide complementary information. Finally, we present an example 2-D application in which sinusoidal signals at multiple frequencies are used as a data source and are inverted to obtain estimates of aquifer heterogeneity. These analyses show the different heterogeneity information that can be obtained from different stimulation frequencies, and that data from several sinusoidal pumping tests can be rapidly inverted using the steady-periodic framework.

Citation: Cardiff, M., T. Bakhos, P. K. Kitanidis, and W. Barrash (2013), Aquifer heterogeneity characterization with oscillatory pumping: Sensitivity analysis and imaging potential, *Water Resour. Res.*, *49*, 5395–5410, doi:10.1002/wrcr.20356.

1. Introduction

[2] It is widely recognized that a major impediment to the successful management and remediation of groundwater is our general lack of knowledge about subsurface properties. Because of the expense required to access most subsurface deposits (especially in deep and/or "hard" aquifer materials), available data is often sparse, and it can be difficult to infer aquifer property distributions between available boreholes. Especially for applications involving transport of contaminants, obtaining more detailed knowledge about spatial subsurface variability in key parameters (primarily hydraulic conductivity, K) is crucial for developing accurate predictive models and designing adequate remediation strategies [*Illman and Alvarez*, 2009; *Anderson and McCray*, 2011].

[3] Another major difficulty in making predictions about aquifer behavior, which remains a persistent challenge for characterization efforts, is the fact that aquifer properties may change considerably, as a result of remedial activities or other processes, and thus all estimates of aquifer properties represent only snapshots whose utility decreases with time. Many processes can alter expected aquifer behavior and are typically encountered during aquifer remediation processes. These include, among others:

[4] 1. The growth of biofilm on sediment grains due to microbial remediation which can significantly alter aquifer hydraulic conductivity, especially near injection wells.

[5] 2. The production of subsurface gases during remediation which can alter the storage properties of aquifer volumes (i.e., by adding compressibility).

[6] 3. Changes to the chemical balances in the subsurface which can cause either precipitation on (or dissolution of) porous media material, also affecting flow and transport parameters.

[7] 4. While not actually altering aquifer material per se, the infiltration of high-kinematic or low-kinematic viscosity

Additional supporting information may be found in the online version of this article.

[1]Department of Geosciences, Boise State University, Boise, Idaho, USA.
[2]Department of Geosciences, University of Wisconsin-Madison, Madison, Wisconsin, USA.
[3]Department of Civil and Environmental Engineering, Stanford University, Stanford, California, USA.

Corresponding author: M. Cardiff, Department of Geoscience, University of Wisconsin-Madison, 1215 W. Dayton Street, Weeks Hall, Madison, WI 53706, USA. (michaelcardiff@boisestate.edu)

0043-1397/13/10.1002/wrcr.20356

fluids into an aquifer volume can alter the "effective" behavior of that volume.

[8] 5. Excess pumping which may lead to compaction of aquifer materials, affecting future storage and conductivity behaviors.

[9] For these reasons, developing aquifer characterization strategies that are cost-effective for repeated and/or continuous implementation will provide valuable information for reducing overall remediation costs.

[10] Estimation of aquifer properties for improving model predictions has been a subject of major research for several decades, and the literature in this area is extensive, covering pressure-based, geophysically based, tracer-based, combination (e.g., geophysical/tracer, or pressure/tracer), and sample-based (coring) methods. A general review of the literature along with a summary of the benefits and drawbacks of each class of methods can be found in *Cardiff et al*. [2012] and (with an emphasis in geophysical methods) in *Rubin and Hubbard* [2005].

[11] Focusing in specific on pressure-based characterization methods, i.e., methods in which changes in head or flow rate provide information content for mapping heterogeneity, several different methods have been advanced for field practice. Fully penetrating, constant rate pumping tests and fully penetrating slug tests are the most prominent characterization methods to date and are relatively easy to implement with minimal equipment, but do not allow the distinction of vertical property variability. A variety of characterization methods have been advanced that are capable of estimating vertical changes in aquifer properties as a tool is advanced, including the partially penetrating slug test [*Bouwer and Rice*, 1976; *Zlotnik and McGuire*, 1998; *Butler*, 1998; *Cardiff et al*., 2011], borehole flowmeter [e.g., *Hess*, 1986, 1989; *Molz et al*., 1994; *Paillet*, 1998], and dipole-flow test [e.g., *Kabala*, 1993; *Zlotnik and Zurbuchen*, 1998]—all utilized in existing wellbores—as well as direct push methods including the direct-push permeameter and direct-push slug testing [e.g., *Butler et al*., 2002; *Dietrich and Leven*, 2009].

[12] Due to existing technical capabilities, data limitations, or equipment limitations, much historical work in aquifer characterization has focused on estimation of bulk aquifer property averages (i.e., assuming homogeneity). When not fitting hydrologic data with homogeneous models, aquifer property variability in one-dimension (1-D)—e.g., by assuming vertically layered strata—is often the only variability examined. However, many recent studies have emphasized the importance of estimating fully three-dimensional (3-D) aquifer property variability, especially in order to make accurate and meaningful predictions about contaminant transport. Traditional hydrologic strategies for extending 1-D insights on aquifer property variability to 3-D volumes generally consist of simple interpolation between measurement locations, which requires dense borehole spacings in order to obtain accurate 3-D estimates.

[13] Recently, aquifer characterization approaches which tomographically analyze pressure data to infer aquifer heterogeneity have also been developed. 3-D hydraulic tomography (HT) is one such characterization approach which jointly analyzes data from a series of partially penetrating constant-rate pumping tests, using tomographic imaging methods (i.e., inversion) to estimate 3-D aquifer parameter distributions. In many approaches to implementation of 3-D HT, estimates of aquifer parameter uncertainty are produced in addition to images of 3-D aquifer parameter distributions. The utility of HT for estimating hydraulic parameters even at a distance between boreholes has been extensively validated for a variety of application areas through 3-D numerical experiments [e.g., *Yeh and Liu*, 2000; *Zhu and Yeh*, 2005; *Cardiff and Barrash*, 2011], two-dimensional (2-D) laboratory studies [e.g., *Illman et al*., 2007; *Liu et al*., 2007], and some recent 3-D transient hydraulic tomography (3-D THT) field experiments [*Berg and Illman*, 2011; *Cardiff et al*., 2012]. A comprehensive summary of other HT research can be found in *Cardiff and Barrash* [2011].

[14] In stimulating the aquifer, almost all hydraulic tomography approaches implemented to date apply a "traditional" constant-rate pumping test (see references in Table 1, *Cardiff and Barrash* [2011]). The tomographic analysis approaches suggested for traditional pumping tests often require either that the pumping test be allowed to run until steady state is approximately achieved (which can be time consuming in the field), or that collected transient data be analyzed using a transient numerical model (which incurs high computational modeling costs). Two notable exceptions are the works of *Bohling et al*. [2002, 2007], who suggested a "steady shape" approach to drawdown analysis and applied this approach to the Geohydrologic Experimental and Monitoring Site (GEMS), and of *Li et al*. [2005], who suggested analyzing temporal moments of drawdown for data compression (an approach later applied to multiple pumping test hydraulic tomography by *Zhu and Yeh* [2006] and *Yin and Illman* [2009]). However, even when clever analysis techniques are used, traditional pumping tests regularly require extraction or injection of significant quantities of water, which may be undesirable or costly at contaminated sites, due to costs associated with pumped water treatment in addition to the fear of significantly altering contamination distributions. Unfortunately, these are often the sites where detailed characterization is of the most interest.

[15] In order to avoid the extraction of significant quantities of water, other hydraulic tomography approaches have been suggested in which short-duration pressure pulses are used as a stimulation [e.g., *Brauchler et al*., 2003, 2007]. In this case, the travel time and amplitude of the observed responses are used as the data source for inversion. Use of this framework allows an inversion in which the pressure wave's travel time and amplitude can be inverted using an asymptotic, curved-ray model [*Vasco et al*., 2000; *Brauchler et al*., 2003]. *Vasco et al*. [2000] has shown how travel time sensitivities can be modeled using curved-ray theory, while noting that amplitude sensitivities are more diffuse, as indicated through their Born sensitivities presented in that work. Pulse tests have advantages over constant-rate pumping tests in that significant quantities of water need not be injected or extracted. However, the distance over which pulse responses can be effectively measured is limited by the hydraulic diffusivity of the aquifer.

[16] Another type of pumping test that has been suggested in the literature is oscillatory pumping. An early example, applied to petroleum reservoir testing, is *Kuo* [1972]. Pressure pulse testing, a related method, has been used in petroleum applications since at least 1970 as well

[*Vela and McKinley*, 1970]. In the hydrogeologic literature, *Black and Kipp* [1981] developed an analytic solution for the steady-periodic response to stimulation by either a point-source or line-source oscillatory stimulation, and analyzed the effective distance over which these signals propagate in various aquifer scenarios. *Bernabe et al*. [2005] advocated the use of oscillating signals for core sample analysis, while emphasizing useful dimensionless groupings for parameter estimation. *Rasmussen et al*. [2003] developed a set of analytic solutions similar to *Black and Kipp* [1981] for oscillatory pressure signal propagation, while adding a semianalytic integral solution for the transient response associated with oscillatory pumping beginning. The authors then applied their solution to characterization of the Savannah River site—responses were fit one at a time via curve matching, resulting in a series of "effective" hydrologic parameter estimates for the aquifer. Other field applications include: *Renner and Messar* [2006], who obtained effective parameter estimates using periodic testing at a field site in Bochum, Germany; *Maineult et al*. [2008], who performed oscillating pumping and observed self-potential geophysical responses at the same site; and *Becker and Guiltinan* [2010], who obtained effective (homogeneous) parameter estimates for a geothermal system in New York, USA by utilizing periodic hydraulic tests. In the petroleum literature, *Hollaender et al*. [2002] summarizes other works in which models were developed for different periodic testing geometries, assuming homogeneous reservoir parameters. Each of the works mentioned above utilized oscillating pumping testing only to obtain effective (i.e., equivalent homogeneous) aquifer parameter values. However, most recently, *McElwee et al*. [2011] utilized an approximate travel time-based approach that assumed wave propagation was affected by heterogeneity only along a straight line between source and receiver.

[17] The idea of using oscillatory signals for characterizing heterogeneity has several advantages relative to other approaches suggested. As there is no net water extraction from or injection into the aquifer throughout an oscillatory test, oscillatory testing avoids possible costs and risks associated with handling and treating significant quantities of contaminated water. Oscillatory testing intuitively should also cause less contaminant plume movement than a constant-rate pumping test when used for characterization. And finally, the use of oscillatory signals of chosen, known frequencies allows responses at monitoring locations to be separated from other hydrologic processes or noises—e.g., evapotranspiration, instrument drift, or measurement noise—through robust signal processing routines for sinusoid extraction.

[18] In this work, we propose the concept of Multifrequency Oscillatory Hydraulic Imaging (M-OHI) in which oscillating pumping tests of several frequencies are used in order to provide information about aquifer heterogeneity, and the responses are analyzed through inverse modeling. M-OHI can be implemented in several unique configurations (see Figure 1):

[19] 1. A single testing arrangement can be implemented, with additional heterogeneity information obtained by leaving all stimulation and observation equipment in place and simply altering the stimulation frequency (Figure 1a);

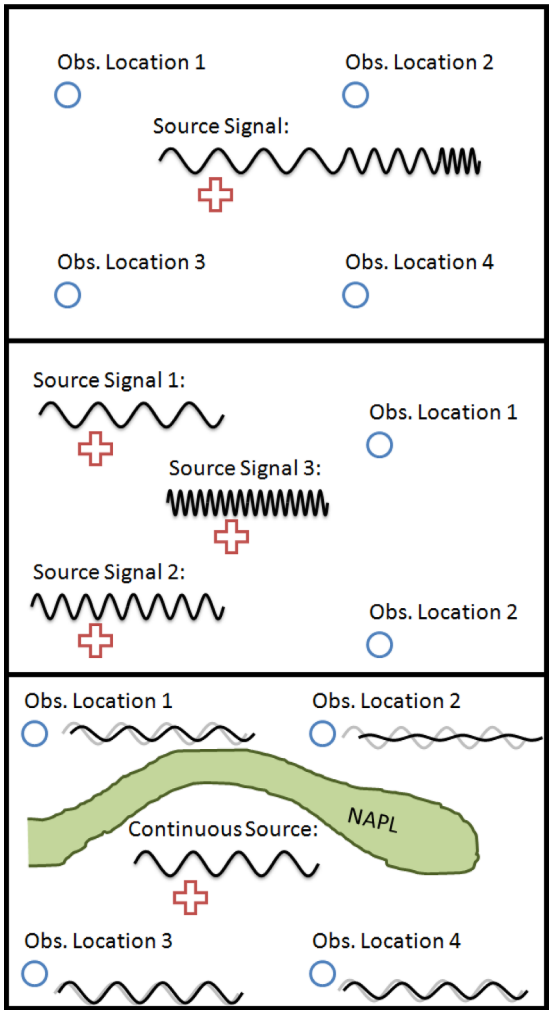

Figure 1. Several methods for performing M-OHI investigations: (a) Single stimulation location with varying frequency source signal, (b) multiple stimulation locations, each with a separate constant-frequency source signal, and (c) long-term monitoring with a constant-frequency source signal and monitored changes in received signals.

[20] 2. Multiple oscillating aquifer stimulations at different locations and frequencies can be performed at once and later separated through frequency-domain decomposition for analysis (Figure 1b); and

[21] 3. Long-term monitoring can be carried out to monitor processes or property changes, without net injection or extraction of water (Figure 1c).

[22] In order to be able to efficiently and accurately interpret multifrequency oscillatory testing data, we propose a mathematical strategy for sensitivity analysis and inversion that utilizes a fast-running steady-periodic numerical framework. We show, through synthetic experiments, that steady-periodic numerical modeling can accurately capture the impact of heterogeneities on oscillatory signal propagation, and can be used for efficient inversion. We first review in section 2 the governing equations for oscillating signals in aquifers and fundamental solutions that have been derived for homogeneous aquifer cases. In section 2.2, we develop an alternate approach—a steady-

periodic or "pseudosteady state" method for analysis of M-OHI data—and show that it is able to predict oscillatory signal response to heterogeneity at a drastically reduced computational cost (relative to fully transient numerical modeling). We then show in section 3 through numerical modeling (validated against analytic solutions) that the straight-ray-based travel time approach for modeling oscillations traveling through heterogeneous media (as used by *McElwee et al*. [2011]) can lead to inaccurate interpretations. Then, in section 4, we extend this model to allow the evaluation of sensitivities using a continuous-form adjoint state formulation, and use this solution to visualize the sensitivity of M-OHI data to spatially distributed aquifer heterogeneity. These sensitivity maps show conclusively that oscillatory signals at different stimulation frequencies effectively "sample" different heterogeneity within the aquifer (assuming the standard governing equations for groundwater flow apply at the given frequency). We finally present an example application in which heterogeneity is imaged using a single testing arrangement with multiple-frequency aquifer stimulations in section 5, and show the additional imaging detail that can be obtained with multi-frequency stimulations. For ease of visualization, the forward and inverse modeling results shown are for 2-D (i.e., fully penetrating) aquifer imaging, though 3-D results are just as easily derived. We conclude and summarize our results in section 6, and provide a discussion of related efforts and areas for future work in section 7.

2. Mathematical Background

2.1. Transient Model

[23] For the purposes of this work, we assume that flow in the aquifer of interest can be modeled as confined (with standard, linear elastic storage) or, if unconfined, can be treated appropriately using a saturated flow model with the standard linearized water table approximation (as used by *Neuman* [1972]). For a domain of interest Ω with boundaries Γ, the governing equations assumed are:

$$S_s \frac{\partial h}{\partial t} = \nabla \cdot (K \nabla h) + q \qquad \forall \mathbf{x} \in \Omega, t \geq 0 \tag{1}$$

$$h = 0 \qquad \forall t \geq 0, \mathbf{x} \in \Gamma_d \tag{2}$$

$$\nabla h \cdot \mathbf{n} = 0 \qquad \forall t \geq 0, \mathbf{x} \in \Gamma_n \tag{3}$$

$$K \nabla h \cdot \mathbf{n} = S_y \frac{\partial h}{\partial t} \qquad \forall t \geq 0, \mathbf{x} \in \Gamma_w \tag{4}$$

where $\mathbf{x}$ is a vector of spatial coordinates $[L]$; t represents time $[T]$; Γ_d, Γ_n, and Γ_w represent Dirichlet, Neumann, and linearized water table boundaries, respectively; $h(\mathbf{x},t)$ is the field variable representing changes in head $[L]$ from an assumed steady initial condition; $S_s(\mathbf{x})$ is a scalar field of specific storage values $[1/L]$; $K(\mathbf{x})$ is a scalar field of hydraulic conductivity values $[L/T]$ (assumed isotropic); $q(\mathbf{x})$ is a scalar field of volumetric water sources $[(L^3/T)/L^3]$; $S_y(\mathbf{x})$ is a scalar field of specific yield values $[-]$; and $\mathbf{n}$ represents the outward normal for a given boundary. For 2-D depth-averaged confined aquifers with horizontal confining layers, we will similarly assume:

$$S \frac{\partial h}{\partial t} = \nabla \cdot (T \nabla h) + q \qquad \forall \mathbf{x} \in \Omega, t \geq 0 \tag{5}$$

$$h = 0 \qquad \forall t \geq 0, \mathbf{x} \in \Gamma_d \tag{6}$$

$$\nabla h \cdot \mathbf{n} = 0 \qquad \forall t \geq 0, \mathbf{x} \in \Gamma_n \tag{7}$$

where S is storativity $[-]$ and T is transmissivity $[L^2/T]$.

[24] To model periodic stimulations, we assume for simplicity that q can be represented as a cosinusoidal source. Representing a single-frequency oscillator in an aquifer can be accomplished by setting:

$$q = Q(\mathbf{x}) \cos(\omega t) \tag{8}$$

where $Q(\mathbf{x})$ is a scalar field giving peak volume flow rates $[(L^3/T)/L^3]$ and ω is the angular frequency of the oscillation [radians/T]. Note that because of the linearity of the governing equations (1)–(4), a multifrequency signal can be decomposed such that several oscillation frequencies (either coming from a single oscillator or from multiple oscillators at different locations) can be modeled separately and then combined (added) to obtain the total response in an aquifer.

2.2. Steady-Periodic Model

[25] The governing equations presented above can be used to model both initial startup behavior of an oscillating pump in an aquifer as well as the eventual long-term response. Still, these simulations require an expensive transient numerical model with short time steps in order to obtain accurate solutions. However, if we neglect the period of start up, during which a truly transient response occurs, we can focus on numerical modeling of the long-term or "steady-periodic" response, which provides a more efficient modeling framework.

2.2.1. Governing Equations

[26] Using Euler's formula, we represent the oscillator (8) as the real part of a complex expression:

$$q = \mathrm{Re}\left[Q(\mathbf{x}) \exp(i\omega t)\right] \tag{9}$$

[27] After a period when the response still depends on initial conditions, the aquifer responds in a steady-periodic fashion. Since the partial differential equation (PDE) under study—as presented in formulas (1)–(4)—is linear, the solution for the response in the aquifer can therefore be represented as the real part of another complex function:

$$h(\mathbf{x}, t) = \mathrm{Re}\left[\Phi_\omega(\mathbf{x}) \exp(i\omega t)\right] \tag{10}$$

where $\Phi_\omega(\mathbf{x})$ is a complex-valued field variable. That is, it is expected that while the phase offset and magnitude of oscillations will vary throughout the domain, the whole domain will respond at the same frequency of the input oscillation. The complex field variable Φ_ω, known as the phasor,

compactly encodes the amplitude and phase-offset of the generated steady-periodic wave at every location in the domain of interest. The subscript ω is used to denote the fact that the phasor solution applies for a particular input frequency, i.e., for each input frequency, a different phasor solution will be obtained. Plugging the above definitions into the governing equation (1) and the boundary conditions (2)–(4) results in:

$$i\omega S_s \Phi_\omega = \nabla \cdot (K \nabla \Phi_\omega) + Q \qquad \forall \mathbf{x} \in \Omega \tag{11}$$

$$\Phi_\omega = 0 \qquad \forall \mathbf{x} \in \Gamma_d \tag{12}$$

$$\nabla \Phi_\omega \cdot \mathbf{n} = 0 \qquad \forall \mathbf{x} \in \Gamma_n \tag{13}$$

$$K \nabla \Phi_\omega \cdot \mathbf{n} = i\omega S_y \Phi_\omega \qquad \forall \mathbf{x} \in \Gamma_w \tag{14}$$

where, because the governing equations must apply for all t, the factor of $\exp(i\omega t)$ has been divided out of all governing equations and boundary conditions [see, e.g., *Townley*, 1993; *Vasco and Karasaki*, 2001]. The solution for the steady-periodic response of h is then the real part of $\Phi_\omega \exp(i\omega t)$, once Φ_ω is found through solution of the above equations. By using measurements of steady-periodic conditions, the benefit of the formulation for $\Phi_\omega(\mathbf{x})$ is that the steady-periodic signal can be modeled using the above complex valued but steady-state formulation, which is much more efficient than full transient modeling of head.

[28] The above formulation is a general form of the transient groundwater flow equations (for oscillating tests) that includes, as a special case, the steady-state response of an aquifer to a constant pumping rate. Note that, as ω approaches 0 (infinite period), the storage term drops out of equations (11)–(14), resulting in the equation for long-term aquifer response to a constant pumping rate. Thus, the steady-periodic governing equations can be used to analyze steady-state pumping tests (and their sensitivity) simply by setting ω equal to 0.

2.2.2. Analytic Solutions

[29] Analytic solutions for steady-periodic groundwater flow can generally be derived only if (1) the source terms (Q) are simple, (2) the flow parameters K and S_s are homogeneous or follow simple structures (e.g., horizontal layering), and (3) the problem domain geometry is amenable (e.g., an infinite domain in 3-D or a 2-D laterally infinite domain with constant finite thickness). However, the fundamental analytic solutions available can be useful when studying the expected signal magnitude observable from such tests, and for deriving first-order approximations of observations' sensitivity to fine-scale heterogeneities.

[30] In particular, for our purposes, the solutions of *Black and Kipp* [1981] provide a useful starting point. Their work investigated two key cases—the steady-periodic response to (1) a point source located within an unbounded, homogeneous, isotropic 3-D aquifer volume with elastic storage and (2) a fully penetrating line source located within a laterally unbounded, but finite thickness, homogeneous isotropic confined aquifer. These solutions provide a useful starting point for studying the information content of partially penetrating and fully penetrating oscillating pumping tests, respectively. As given in that work, the solutions for these two cases are the real part of the following complex functions:

$$\text{Point Source} : \left[\frac{Q}{4\pi K r}\exp\left(-\left(\frac{1+i}{2^{1/2}}\right)\left(\frac{\omega S_s r^2}{K}\right)^{1/2}\right)\right]\exp(i\omega t) \tag{15}$$

$$\text{Line Source} : \left[\frac{Q}{2\pi K b}K_0\left(\left(\frac{\omega r^2 S_s}{K}\right)^{1/2}\exp(i\pi/4)\right)\right]\exp(i\omega t) \tag{16}$$

where r is radial distance from the oscillator [L]. For the line source case, K_0 represents the modified Bessel function of the second kind and b represents the confined aquifer thickness [L]. In these formulas, the portion of the solution in square brackets represents the solution for Φ_ω as defined above, in a homogeneous semi-infinite domain with the given source terms.

3. Numerical Analysis

[31] In addition to their use for providing estimates of effective aquifer properties (i.e., if homogeneity is assumed for a particular test response), the analytic solutions above provide a validation tool for numerical modeling of oscillatory tests. Here, we develop a numerical model for simulating oscillatory flow through a 2-D, depth averaged, heterogeneous confined aquifer, and use this model to investigate the effects of heterogeneities on observed responses. For the homogeneous test case, the key goal of the analysis is to show the eventual convergence of transient response to a steady-periodic response and thus validate our implementation of the phasor-based (steady-periodic) numerical model. For the heterogeneous test case, the goals of the modeling results are twofold. First, our heterogeneous test cases validate that the use of a phasor-based model for simulating heterogeneous aquifer response matches the long-term response seen in fully transient models. Second, the heterogoneous test cases provide a method to compare the accuracy of our approach for M-OHI analysis against the analysis suggested by *McElwee et al*. [2011].

[32] For all analyses in this section, we utilized the well-tested, commercial finite element-based COMSOL Multiphysics modeling software (version 4.2a, *COMSOL AB* [2011]), and simulate several scenarios using the software's "Darcy's Law" flow module. To facilitate discussion and exploration using these models, all models and results are made available as part of the supporting information associated with this paper.

3.1. Model Description

[33] The numerical modeling geometry for our first set of synthetic modeling experiments is shown in Figure 2. To approximate a semi-infinite 2-D scenario, a large disc is utilized as the modeling domain. A point at the origin serves as an oscillating volume flow rate source, and observations are recorded as output at distances of 2, 4, 6, and 8 m (labeled N1, N2, F1, and F2, representing near and far locations, respectively). In addition to the large-scale geometry, a set of square 1 m × 1 m areas (see Figure 2,

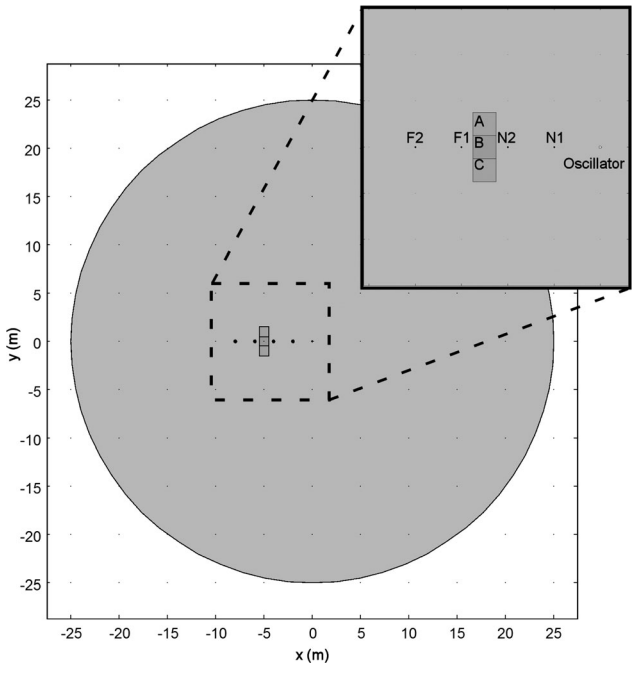

Figure 2. Geometry of the modeling domain for the sample problem investigated with COMSOL. Inset shows magnification of the central modeling area, including oscillator stimulation location, observation locations (N1, N2, F1, and F2), and areas where heterogeneities were implemented (areas A–C).

inset, labeled A, B, C) are defined centered at 5 m from the oscillator, where hydraulic conductivity values can be modified to examine the effects of aquifer heterogeneity. Throughout, we assume an oscillator with a period of 20 s and a peak volume flow rate of $1.26e{-}3$ m^3/s (roughly 80 L/min). Below we examine both homogeneous test cases and heterogeneous test cases in which we reduce the K in the 1 m^2 areas by an order of magnitude. In all cases, the transient numerical model contained about 7000 elements, used a maximum time step of 1% of a period, and required roughly 2–3 min to run on a standard desktop PC.

3.2. Transient Homogeneous Test Case

[34] In the first modeling case, the squares A, B, and C were set to have the same conductivity and storage parameters as the rest of the aquifer. We then simulate oscillating pumping in the aquifer, using a pumping stimulation that contains a period of "ramp-up" in order to minimize propagation of early time transients. Specifically, the source at the pumping well used is:

$$q(t) = Q\cos(\omega t) \times \left(1 - \exp\left(-t/t_{\text{ramp}}\right)\right) \tag{17}$$

where, for this case, t_{ramp} was set to the period of the oscillation, 20 s. We compare the results of this model (i.e., the response at all observation locations) against the analytic 2-D steady-periodic solution (16) in Figure 3, and find excellent agreement after initially transients have subsided, roughly after about five periods. In particular, both the amplitude and phase of the sinusoids returned by the transient numerical model match the analytic solution once steady-periodic conditions are obtained. This line of testing, along with other checks on mass balances and model convergence criteria, help to validate the numerical model for further use.

3.3. Transient Heterogeneous Test Cases

[35] We next performed several heterogeneous numerical simulations in order to understand the response of oscillatory signals to aquifer heterogeneity. Throughout we utilize a shortened naming convention to describe these models; "AC Heterogeneity," for example refers to a test case in which K in areas A and C has been lowered by an order of magnitude. We consider three test cases with heterogeneity—AC, B, and ABC heterogeneity, and compare the results with what would be expected under the straight-ray-based tomographic approach suggested by *McElwee et al*. [2011]. The results of these numerical investigations, shown in Figure 4 as four subplots (one per observation well), provide interesting insights into the response of oscillatory flow to heterogeneities. In each case, a single period of the response is shown starting at 100 s (five periods) after the aquifer stimulation begins.

[36] The first notable result, which is inconsistent with a straight-ray-based approximation of oscillation travel times, is that heterogeneities need not be between the pumping and observation location to affect response. Figure 4 clearly shows that in all heterogeneous test cases, response at wells N1 and, especially, N2 are affected by heterogeneities A, B, and C, which are not along a path between these observation wells and the pumping well. The amplitude of the response at N2 in particular is increased dramatically relative to the homogeneous base case, which could be misinterpreted as a high-K heterogeneity existing between N2 and the pumping well if the straight-ray-based approximation were used (e.g., the method of *McElwee et al*. [2011]). The second notable result is that, even at wells on the opposite side of the heterogeneities (F1 and F2), the response at these wells is governed not only by the heterogeneity in region B but also by regions A and C, which do not fall along a straight path between the pumping well and these observation locations. In fact, at both F1 and F2, the response to B heterogeneity is very similar to the response of AC heterogeneity. Thus, AC heterogeneity could lead to a misinterpretation that there was a low-K inclusion directly between the pumping well and the far observation locations. Finally, a comparison between B heterogeneity and ABC heterogeneity response further emphasizes the support volume of oscillatory measurements, which extends beyond the ray between pumping and observation location. In all four cases—but most especially at N2, F1, and F2—the change in response relative to the homogeneous base case is much larger if K is reduced in the larger volume ABC than if it is simply reduced in region B. Again, interpretation of the ABC results using ray-based approximations suggested to date would predict an overly low-K inclusion, especially at F1 and F2 where a large decrease in observed amplitude and large increase in the phase offset are seen.

3.4. Discussion of Transient Modeling Results

[37] It has been shown through several methods, including adjoint state-based sensitivity analyses [e.g., *Oliver*,

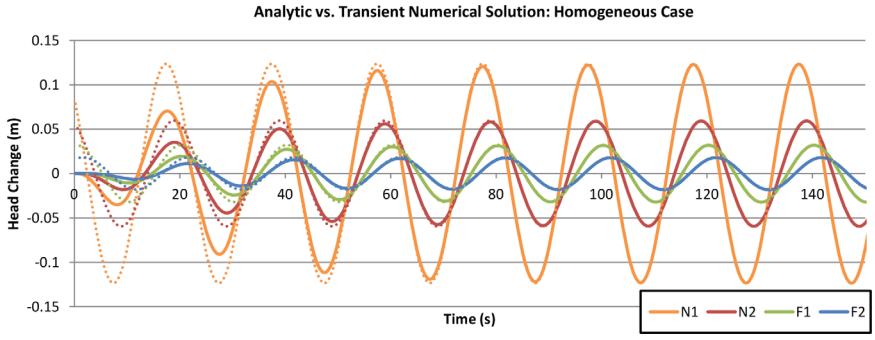

Figure 3. Comparison between steady-periodic analytic solution (dashed lines) and homogeneous COMSOL numerical simulation (solid lines) solved in a transient model.

1993; *Wu et al*., 2005; *Leven and Dietrich*, 2006; *Vasco and Karasaki*, 2006; *Huang et al*., 2011], that response at monitoring wells to pumping is highly sensitive to near-well conductivity values, but also sensitive to hydraulic conductivity variability within a large support volume around both pumping and observation well. In addition, due to the diffusion-based physics of the groundwater flow equations, pumping test responses experience both "positive" sensitivity to aquifer parameters between the source and receiver, as well as "negative" sensitivity in the immediately opposite directions of both the source and receiver. It is thus not surprising that straight-ray-based approximations to the true groundwater flow equations may be insufficient to simulate observed response; these models do not take advantage of the full information content provided by the governing physics of the groundwater flow equation.

[38] While the fundamental physics for oscillatory signal propagation in aquifers may not be accurately modeled by straight-ray-based approximations, in certain scenarios the use of approximate straight-ray-based models may be advantageous in that the models have drastically reduced computational costs relative to fully transient groundwater flow simulators, and may represent enough of the underlying physics to be used in inverse modeling frameworks to produce reasonable tomography results. In terms of analyzing oscillating pumping tests' long-term response, our modeling suggests that use of the straight-ray-based approximation for long-term response (as performed by *McElwee et al*. [2011]) can introduce inaccuracies. A more physically accurate ray-based model could be applied, which takes into account ray bending due to heterogeneity and the diffuse sensitivity of wave amplitudes to heterogeneity, as advocated by *Vasco et al*. [2000]. Alternately, the steady-periodic modeling approach discussed above is physically exact—being derived from the fundamental Darcy-based groundwater flow equations—and is able to

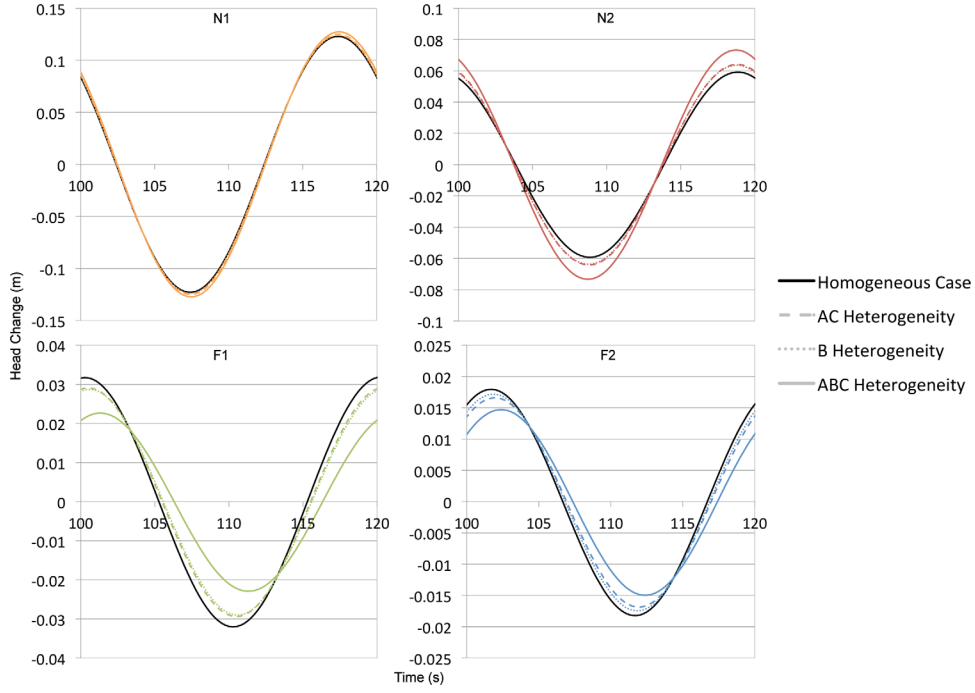

Figure 4. Changes in measured response oscillations for heterogeneity scenarios relative to homogeneous base case (note, both amplitude and phase changes).

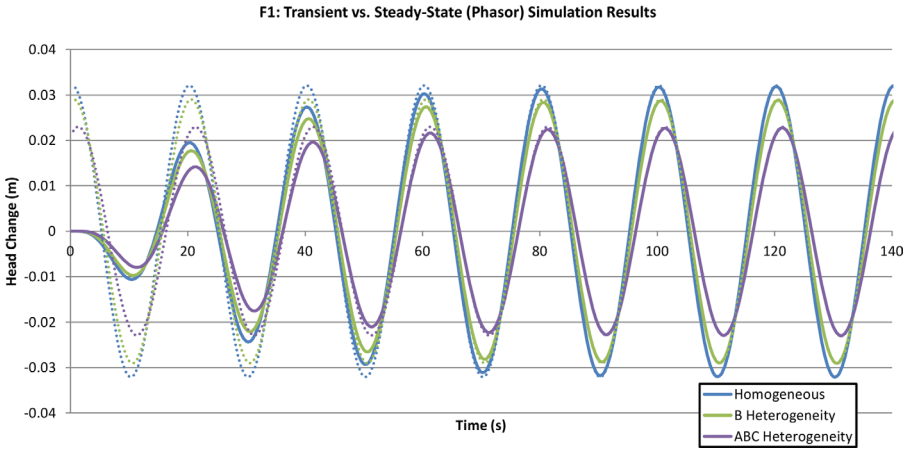

Figure 5. Comparison between numerical simulation results obtained at location F1 under various heterogeneous cases. Dashed line represents steady-periodic solution derived from phasor numerical results. Solid line represents transient simulation results.

realize computational savings by resulting in a modeling framework that is, effectively, steady state.

3.5. Steady-Periodic Modeling

[39] To validate our phasor-based approach for heterogeneous models, we utilized the multiphysics interface of COMSOL to add a custom "physics" (defining the phasor governing equations) to our existing numerical model described in section 3. In COMSOL, this means that a new set of governing equations were applied to the model—using the same model geometry and finite element discretization—and were then discretized to a finite element form and solved by COMSOL. We then ran the numerical model for all test cases described above, including the homogeneous base case, along with B, AC, and ABC heterogeneity cases.

[40] The transient numerical model discussed earlier and implemented in COMSOL solved from $t = 0$ s to $t = 200$ s, or 10 periods, and routinely required between 2 and 3 min to solve on a modern desktop PC. In contrast, the steady-periodic phasor-based model with the same discretization routinely required only between 2 and 4 s to solve. Thus, even though COMSOL was required to solve for a complex-valued field variable in the phasor formulation, significant speed gains are realized due to the fact that the phasor-based model is steady state. Once the complex phasor field variable is solved for using the numerical model, the solution (representing steady-periodic response) can be converted into a transient sinusoidal signal for comparison against transient solutions by computing the real part of equation (10). Accuracy of the phasor-based model was validated by comparing these results against the fully transient numerical solutions described earlier. A sample of the results is shown in Figure 5, which compares the simulated observations from the earlier transient model against the steady-periodic sinusoid derived by using the phasor-based simulation. As can be seen, in both the homogeneous and heterogeneous analysis cases, the steady-periodic phasor-based solution produces results that are indistinguishable from the earlier modeling results after initial transients subside (again, after ≈5 periods from start up).

4. Multifrequency Oscillatory Hydraulic Imaging Sensitivity Analysis

[41] As mentioned in section 1, steady-periodic models for oscillatory flow have been used to estimate effective homogenous aquifer properties [e.g., *Rasmussen et al*., 2003]. To the best of our knowledge, however, the sensitivity of these signals to spatially distributed hydrologic parameters has not been investigated rigorously, and thus it is unclear what spatial averaging is obtained by analysis of such signals. Similarly, to date the use of such signals at multiple frequencies for aquifer imaging has not been investigated. Below we analytically derive expressions that can be used to compute the sensitivity of a steady-periodic signal to spatially distributed aquifer parameters using the adjoint state method. Given the assumed governing equations for groundwater flow, this represents a physically accurate and exact method for computing sensitivities of signal parameters (amplitude and phase) to distributed aquifer parameters (K, S_s, and S_y).

4.1. Adjoint State Equations

[42] In order to use oscillatory pressure stimulations for imaging of aquifer heterogeneity (i.e., for inverse modeling), it is necessary to be able to evaluate the local sensitivity of measured signal characteristics (e.g., amplitude and phase offset) to spatial variability in the key aquifer parameters of interest K, S_s, and S_y. During inversion, we generally have a large set of I measurements stored in a vector $\mathbf{m} = [m_1, m_2 . m_I]^T$ and a large set of J parameters we are trying to estimate, stored in a vector $\mathbf{p} = [p_1, p_2, \ldots, p_J]^T$. For example, p_j could represent the value of the hydraulic conductivity in the jth cell of a numerical model.

[43] Generally in inverse modeling, we would like to calculate a Jacobian matrix $\mathbf{H}$ with elements $\mathbf{H}_{i,j} = \frac{\partial m_i}{\partial p_j}$ for all i and j. A simple way to estimate these sensitivities would be via numerical finite difference approximations, i.e., by varying each element of $\mathbf{p}$ one-at-a-time by some small amount Δp_j and approximating:

$$\left.\frac{\partial \mathbf{m}}{\partial p_j}\right|_{\tilde{\mathbf{p}}} \approx \frac{\mathbf{m}(\tilde{\mathbf{p}} + \Delta p_j) - \mathbf{m}(\tilde{\mathbf{p}})}{\Delta p_j} \tag{18}$$

where $\tilde{\mathbf{p}}$ represents the local value of $\mathbf{p}$ at which sensitivities are being calculated. Calculating the measurements $\mathbf{m}$ means that the forward model must be run using each set of parameter values, thus this method requires at least $J+1$ forward model runs—one run to evaluate the value of all measurements at the local value $\mathbf{m}(\tilde{\mathbf{p}})$, and J runs to evaluate the measurement vector for each perturbation $\mathbf{m}(\tilde{\mathbf{p}} + \Delta p_j)$. This can be thought of as calculating the Jacobian matrix by obtaining one column per model run.

[44] The adjoint state method is another method for deriving measurement sensitivities. By analytically manipulating the governing equations and measurement definitions, one can arrive at an equivalent set of computations that produce the Jacobian matrix through only one forward run and I adjoint model runs. The adjoint model runs generally require equal computing time to a forward model run, thus the adjoint method essentially requires at most $I+1$ model runs. This method is therefore much more efficient when the number of measurements is much smaller than the number of parameters to be estimated, as is often the case in spatially distributed parameter estimation problems. The adjoint method can be thought of as calculating the Jacobian matrix by obtaining one row per adjoint run.

[45] The adjoint state equations can be derived either using discrete matrix manipulations [e.g., *Townley and Wilson*, 1985] or by analytic manipulations of the governing PDEs. The discrete method is often useful for programming an adjoint state computation into an existing numerical model. However, generally greater physical insight is gained by deriving the adjoint state equations in a continuous, PDE-based form. This was the method presented in *Cardiff and Kitanidis* [2008], where a generalized adjoint state for a linear, second-order in space PDE was derived. The formulas governing steady-periodic aquifer response (equations (11)–(14)) involve complex numbers but are equivalent to those presented in *Cardiff and Kitanidis* [2008], meaning that the adjoint state sensitivity calculations can be derived simply by using the key formulas and tables presented in that work. For instructive purposes, though, we present a derivation of adjoint state sensitivities for the steady-periodic model in supporting information

[46] To apply the adjoint state approach to the complex-valued, steady periodic governing equations (11)–(14), it turns out that two conditions must be met.

[47] 1. The measurement of the signal can be represented as an integral of some complex-valued "test function" over the modeling domain, i.e., for a single measurement m_i, a test function r_i can be defined such that:

$$m_i = \int_\Omega r_i(\Phi_\omega) d\Omega \tag{19}$$

[48] 2. The test function r_i must be complex differentiable with respect to Φ_ω, i.e., it must satisfy the Cauchy-Riemann conditions.

[49] If we are describing measurements of sinusoids in terms of the amplitude and phase at particular points in space, then the following is an example of an acceptable test function that satisfies the necessary conditions given above:

$$r_i = \left[\ln\left(\left(a^2+b^2\right)^{1/2}\right) + i \arctan\left(b/a\right)\right]\delta(\mathbf{x}-\mathbf{x}_i) \tag{20}$$

where a and b are the real part and imaginary part of Φ_ω, respectively. It is easy to show that, if the head signal measured at a point in space $\mathbf{x}_i$ is $h(\mathbf{x}_i) = \mathrm{Re}\left[(a+bi)\cos(\omega t)\right]$, the log-amplitude and phase offset of the signal are equal to the real and imaginary components of the r_i defined in equation (20), respectively. From here on, we refer to the amplitude of the signal as $M = (a^2+b^2)^{1/2}$, and the phase-offset as $\theta = \arctan(b/a)$.

[50] The key result of the adjoint state derivation presented in supporting information is that the sensitivity of a measurement to hydraulic parameters can be obtained as follows:

[51] 1. Perform a forward model run, solving the governing equations for Φ_ω (equations (11)–(14)) using the current estimates of the parameters $\mathbf{p}$.

[52] 2. For measurement i, perform an adjoint model run, solving the following governing equations for the "adjoint variable" ψ_i using the current estimates of the parameters $\mathbf{p}$:

$$i\omega S_s \psi_i = \nabla\cdot(K\nabla\psi_i) - \frac{\partial r_i}{\partial \Phi_\omega} \qquad \forall \mathbf{x} \in \Omega \tag{21}$$

$$\psi_i = 0 \qquad \forall \mathbf{x} \in \Gamma_d \tag{22}$$

$$\nabla\psi_i \cdot \mathbf{n} = 0 \qquad \forall \mathbf{x} \in \Gamma_n \tag{23}$$

$$K\nabla\psi_i \cdot \mathbf{n} = i\omega S_y \psi_i \qquad \forall \mathbf{x} \in \Gamma_w \tag{24}$$

[53] 3. Calculate $\frac{\partial m_i}{\partial p_j}$ for all j by carrying out the measurement sensitivity integral:

$$\frac{\partial m_i}{\partial p_j} = \int_\Omega \frac{\partial r}{\partial p_j} + \psi_i\left[i\omega\frac{\partial S_s}{\partial p_j}\Phi_\omega - \frac{\partial Q}{\partial p_j}\right] + \frac{\partial K}{\partial p_j}\nabla\Phi_\omega\cdot\nabla\psi_i d\Omega - \int_{\Gamma_w}\psi_i\left(i\omega\frac{\partial S_y}{\partial p_j}\Phi_\omega\right)d\Gamma \tag{25}$$

[54] A similar result for the case of 2-D confined aquifers can be derived by simply replacing S_s with S, replacing K with T, and eliminating water table boundary conditions. The most important point to be noted is that only the measurement integral equation (25) is dependent on the parameter j being investigated. Thus, after performing steps 1 and 2, the sensitivity of one measurement to all parameters can be calculated by repeatedly evaluating this integral for each j without repeating any model runs.

[55] As we have noted earlier, the steady-periodic results presented here can be directly compared against steady-state analyses by setting ω equal to zero. In this case, the forward model (equations (11)–(14)) will contain no storage term (and thus no imaginary phasor components) and the associated adjoint state governing equations presented above will likewise have no imaginary components.

4.2. Sensitivity Visualization

[56] A useful first-order metric for understanding the sensitivity of measurements to spatially distributed parameters is Jacobian visualization [e.g., *Oliver*, 1993; *Leven and Dietrich*, 2006; *Cardiff et al.*, 2009], also known as sensitivity coefficient visualization. For example, in the case of a seismic travel time measurement linearized around a

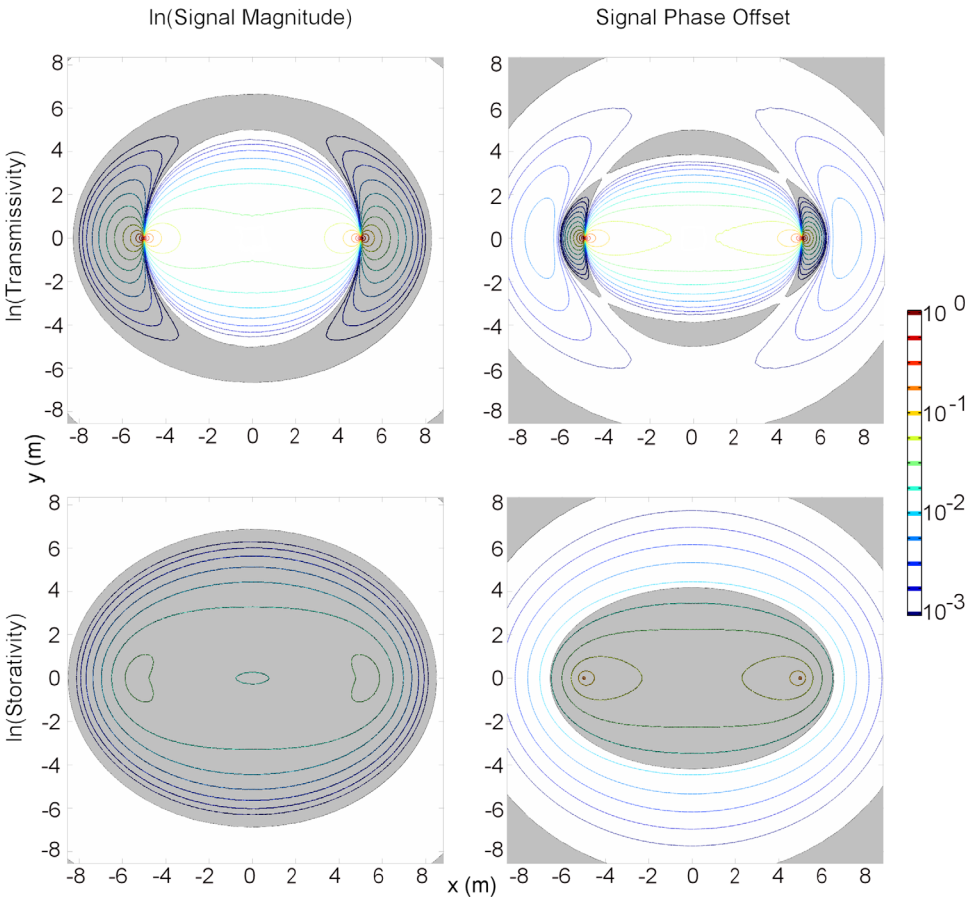

Figure 6. Sensitivity visualization for synthetic aquifer, stimulation period of 10 s. Background color indicates sign of sensitivity (positive or negative), and contours indicate absolute magnitude. Magnitude is unitless in left column, due to using sensitivity of log-Magnitude to log-parameters. Magnitude has units of radians in right column.

homogeneous medium starting model, sensitivity visualization would show that a measurement of travel time has sensitivity to aquifer parameters along a raypath between the stimulation source and the receiver, but is insensitive everywhere else in the domain. In this section, we visualize the linearized sensitivity of an observation to spatially distributed aquifer heterogeneity in a 2-D confined depth-averaged case again using COMSOL as the numerical model. As the visualization is 2-D, the sensitivity is with respect to transmissivity T (equal to K times aquifer thickness for a homogeneous aquifer) and storativity S (equal to S_s times aquifer thickness for a homogeneous aquifer). We assume an observation consists of the amplitude and phase of a signal at a point, i.e., we calculate sensitivity for the observation integrand discussed in equation (20).

[57] As a relevant example, we assume two wells separated by a distance $r = 10$ m, where the pumping well is located at (r/2,0) and the observation well is located at ($-r$/2,0). We linearize the sensitivity for the case of a homogeneous, 2-D aquifer with $K = 1e-5m/s, S_s = 5e-6m^{-1}$ and an aquifer thickness of 15 m. Maximum flow rate for the oscillator is assumed at ≈1 l/s, and constant-head boundaries are assumed at a relatively long distance from the origin. We solve for both the phasor and the adjoint state variable associated with this observation setup in COMSOL, and then calculate the sensitivity field for the observations relative to the T and S field (i.e., the spatial integrand from equation (25)) as follows:

$$H_{\ln M,\ln T}(\mathbf{x}) = \mathrm{Re}\left(T\nabla\Phi_\omega \cdot \nabla\psi_i\right) \tag{26}$$

$$H_{\ln M,\ln S}(\mathbf{x}) = \mathrm{Re}\left(\psi_i i\omega S\Phi_\omega\right) \tag{27}$$

$$H_{\theta,\ln T}(\mathbf{x}) = \mathrm{Im}\left(T\nabla\Phi_\omega \cdot \nabla\psi_i\right) \tag{28}$$

$$H_{\theta,\ln S}(\mathbf{x}) = \mathrm{Im}\left(\psi_i i\omega S\Phi_\omega\right) \tag{29}$$

where $H_{\ln M,\ln T}$ represents the sensitivity field of ln(M) to ln(T).

[58] In Figure 6, we show the observation's amplitude and phase sensitivity to spatially distributed aquifer transmissivity, T (top row) and aquifer storativity, S (bottom row). In particular, it is notable and useful that the amplitude sensitivity structures are different from the phase sensitivity structures. This demonstrates that a single observation of a sinusoidal signal thus provides two pieces of complementary information about aquifer heterogeneity in T and similarly two pieces of complementary information about heterogeneity in S. Similar maps of sensitivity structures are shown in Figure 7 for a case where the signal frequency has been decreased by a factor of five. All four

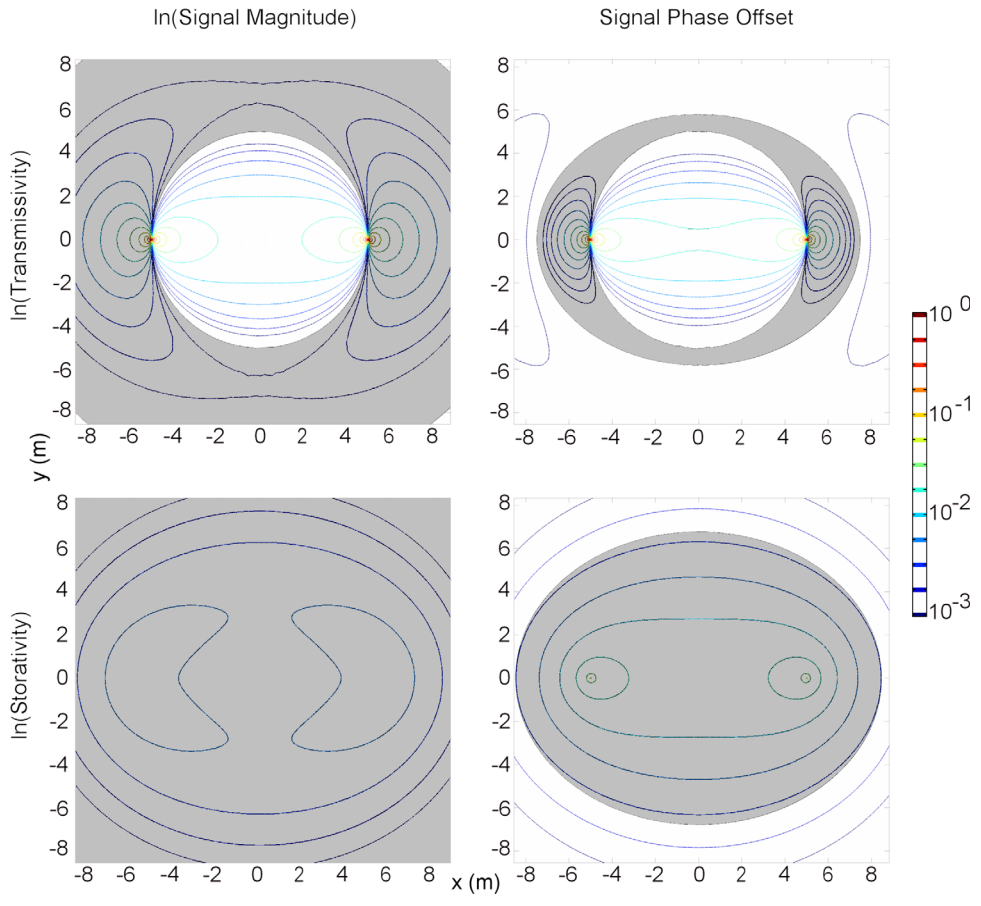

Figure 7. Sensitivity visualization for synthetic aquifer, stimulation period of 50 s. Background color indicates sign of sensitivity (positive or negative), and contours indicate absolute magnitude. Note significant difference from sensitivities obtained at 10 s period. Magnitude is unitless in left column, due to using sensitivity of log-Magnitude to log-parameters. Magnitude has units of radians in right column.

sensitivity structures are different from what is seen in Figure 6, and generally appear to be more spread throughout the domain, suggesting that lower frequency oscillations provide more information about large-scale features, whereas small-scale oscillations are more sensitive to near-field features especially between the pumping and observation locations. In addition, the difference between the structures in Figure 6 versus Figure 7 implies that additional information about aquifer heterogeneity can be obtained by altering the frequency of the aquifer stimulation when using M-OHI. In contrast, sensitivity structures associated with steady state response to constant-rate pumping tests can only be altered by moving pumping or observation locations.

[59] The differences in the sensitivity structure found at different frequencies provide a plausible explanation for what *Renner and Messar* [2006] call the "intrinsic period dependence of [effective] hydraulic properties," a phenomena also observed by *Becker and Guiltinan* [2010]. Since different frequencies of oscillatory testing effectively average over different volumes, this intrinsic period dependence of the effective parameters obtained in their work may simply be a manifestation of subsurface heterogeneity and the differing sensitivities of different frequencies to parts of the aquifer volume. In the case of a homogeneous aquifer analyzed with a homogeneous model, it has been stated that "harmonic testing does not provide more information on the reservoir than conventional well tests" [*Hollaender et al.*, 2002]. However, these conclusions were drawn based on the underlying assumption that the reservoir or aquifer under study has a constant, homogeneous set of parameters to be estimated. In the case of a heterogeneous aquifer, the differing sensitivity maps at differing frequencies clearly show that multiple-frequency oscillatory stimulations can provide additional information about heterogeneity.

[60] The sensitivity maps presented above can be directly compared against sensitivity maps for steady state, constant-rate pumping tests, by using the zero-frequency limit approach discussed earlier. In this case, the only sensitivity with nonzero components will be the sensitivity of log-amplitude to transmissivity. Thus, it is apparent that the steady response to constant pumping is exactly the same as a zero-frequency oscillatory pumping test, and additional sensitivity to heterogeneity can be obtained by performing nonzero-frequency tests, which have observably different sensitivity structures. This is similar to the reason why it is often suggested to analyze transient data from a constant-rate pumping test (instead of only steady state data) for inversion.

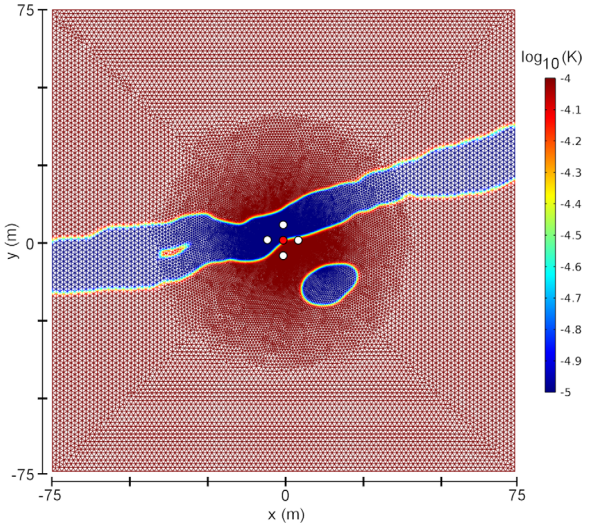

Figure 8. Mesh and heterogeneity used in example imaging problem. Color of mesh indicates model's true $\log_{10}(K)$ value. Dots indicate location of pumping wells (red) and observation wells (white).

Table 1. Relevant Modeling and Inversion Parameters for Imaging Example Application

Parameter	Value
Maximum pumping rate during period	All periods: 1.26 L/s
Maximum head change at observation wells	5 s period: 4.9 cm 10 s period: 8.9 cm 20 s period: 14.1 cm 100 s period: 32.0 cm 200 s period: 41.6 cm 300 s period: 47.2 cm
Size of modeling domain	150 m × 150 m (square)
Aquifer thickness used	15 m
Specific Storage	1E-5 m^{-1}
Finite element mesh setup	Full Mesh: 60,682 triangular elements Largest element size allowed: 1.5 m^2 Element size near wells: 0.15 m^2 Maximum element growth rate: 1.03
Covariance assumed for log10(K)	Linear variogram
Variogram parameters assumed for log10(K)	Slope: 0.01
Measurement error variance	1 cm^2

5. Multifrequency Imaging Example Application

[61] The sensitivity maps presented suggest that additional information about aquifer heterogeneity can be obtained by using multiple frequencies of aquifer stimulations. To demonstrate the improvement in imaging seen when using multiple frequency stimulations versus a single frequency, we present an application of multi-frequency oscillatory hydraulic imaging using our proposed modeling approach. A sample synthetic problem is investigated, with geometry and discretization as shown in Figure 8. The main features of this model are a single pumping well (located at the origin), four surrounding observation wells at distances of 5 m each, and constant-head boundary conditions at a distance from the origin. Other parameters related to the model geometry and pumping stimulation are shown in Table 1. While we test the ability of oscillatory signals to image transmissivity heterogeneity, for simplification in this work we have assumed that storativity is constant throughout the aquifer. In addition, we note that we have chosen to use a single pumping location in this example in order to highlight the comparative improvement of aquifer imaging from single-frequency versus multiple-frequency inversions. However, it should be noted that our approach is in no way limited to single stimulation locations—this is simply a choice used to highlight a particular feature of the analysis framework.

[62] Boundary effects on the problem were minimized by placing constant head boundaries at a distance of 75 m from the origin. To verify that boundary effects were minimal, we populated the model with a homogeneous hydraulic conductivity value of $1e-4$ m/s, and compared the obtained steady-periodic solution at all frequencies against the line-source analytic solution of *Black and Kipp* [1981]. In all cases (i.e., for all frequencies), the measured response amplitudes experienced less than 1 mm difference from the analytic solution.

[63] After model validation, the heterogeneity pattern shown as the mesh color in Figure 8 was imported into the model, and pumping was simulated at the central fully penetrating well (at the origin) at periods of 5, 10, 20, 100, 200, and 300 s. Synthetic data were generated by simulating 1 h worth of steady-periodic aquifer response, with a sampling frequency of 1 Hz, at each stimulation frequency. Response signals were measured at the four fully penetrating observation wells to the north, south, east, and west (each at a distance of 5 m). The records of temporal pressure changes at each well were then contaminated with random white noise with a standard deviation of 1 cm. Examples of the raw data after addition of noise are shown in Figure 9.

[64] To perform inversion, the hour-long record of data from each well at each frequency was first processed using a Bayesian processing routine (which allows propagation of measurement error) to extract the coefficients for the sinusoidal and cosinusoidal components of the observed signal. In essence, the approach consisted of assuming that the time series of data at each point can be represented as:

$$\mathbf{d} = A_\omega \sin(\omega \mathbf{t}) + B_\omega \cos(\omega \mathbf{t}) + \varepsilon \tag{30}$$

where $\mathbf{d}$ represents the data vector at a particular measurement point and frequency; $\mathbf{t}$ is the vector of measurement times; A_ω and B_ω represent the sinusoidal and cosinusoidal coefficients, respectively; and ε is a vector of noise. In the matrix-vector form, the system of equations can be written as:

$$\begin{bmatrix} d_1 \\ d_2 \\ \vdots \\ d_n \end{bmatrix} = \begin{bmatrix} \sin(\omega t_1) & \cos(\omega t_1) \\ \sin(\omega t_2) & \cos(\omega t_2) \\ \vdots & \vdots \\ \sin(\omega t_n) & \cos(\omega t_n) \end{bmatrix} \begin{bmatrix} A_\omega \\ B_\omega \end{bmatrix} + \varepsilon \tag{31}$$

[65] Using this formulation the error in measured time series can be converted into error in the coefficients A_ω and B_ω using the normal equations and standard linear error propagation.

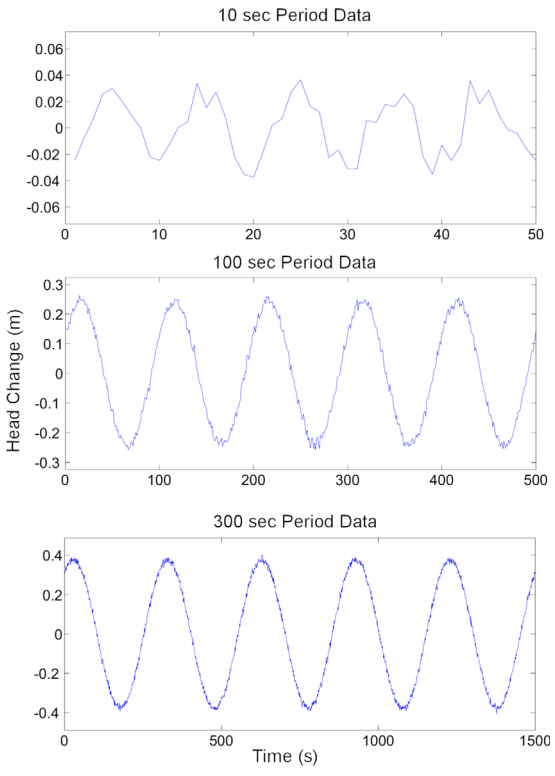

Figure 9. Examples of raw data used in inversions. Figure shows noisy records from North observation well at three different stimulation periods (10, 100, and 300 s periods).

[66] In terms of our inversion approach, we first obtain estimates of A_ω and B_ω by processing the raw (temporal) data using the normal equations and linear error propagation. This provides estimates of "measured" sinusoidal and cosinusoidal coefficients at each stimulation frequency, along with the covariance matrix of the errors of these coefficients. The estimated sinusoidal/cosinusoidal coefficients and their associated measurement errors were then used within a Bayesian geostatistical inverse code (based on the formulation of *Kitanidis* [1995]) in order to invert for heterogeneity in aquifer transmissivity. The objective function optimized is:

$$\min_{\mathbf{s},\beta} \frac{1}{2}(\mathbf{y}-\mathbf{h}(\mathbf{s}))^T\mathbf{R}^{-1}(\mathbf{y}-\mathbf{h}(\mathbf{s})) + \frac{1}{2}(\mathbf{s}-\mathbf{X}\beta)^T\mathbf{Q}^{-1}(\mathbf{s}-\mathbf{X}\beta) \tag{32}$$

where $\mathbf{s}$ is the vector of parameter values (transmissivities), $\mathbf{y}$ is the vector of data (sinusoidal and cosinusoidal coefficients measured at each location at each frequency), $\mathbf{h}()$ is the forward model, $\mathbf{R}$ is the covariance matrix of data errors (derived from the covariance matrix of sinusoidal/cosinusoidal coefficient errors from the normal equations), $\mathbf{X}$ is a vector of drift function values, β is a vector of drift coefficients, and $\mathbf{Q}$ is the expected parameter covariance. In the example, we assumed a priori that the random field was a stationary, constant-mean random field with a linear variogram having a slope of 0.01. This means that $\mathbf{X}$ is a simple vector of ones, and $\mathbf{Q}$ was generated as a generalized covariance equal to -0.01 times the distance between each pair of parameter locations.

[67] In Figure 10, we show the results of aquifer imaging when each frequency is used individually, as compared with the imaging results obtained when multiple frequencies are jointly inverted. As is clearly visible, the use of multiple frequencies for imaging improves the results of imaging. This can also be shown quantitatively, as given in the statistics shown in Table 2. In particular, we note that high-frequency data is only able to accurately image the near field (Figure 10, top left), while low-frequency data provides more "fuzzy" information over a broader spatial extent (Figure 10, bottom left). The combination of appropriate frequencies effectively combines the benefits of each frequency, producing imaging results that are able to more accurately image heterogeneity, even beyond the immediate location of the well field (Figure 10, second column and middle right).

6. Conclusions

[68] Oscillating pumping tests have several advantages relative to traditional, constant-rate pumping tests. However, to date, the use of oscillatory pumping tests for characterizing heterogeneity has been precluded by a lack of studies demonstrating the sensitivity of oscillatory signals to spatially distributed aquifer heterogeneity. In addition, there have been no studies of the ability of multifrequency oscillatory pumping tests to image aquifer heterogeneity.

[69] In this study, by combining the steady-periodic model for oscillatory aquifer flow with an adjoint state-based sensitivity analysis, we were able to derive sensitivity maps that relate metrics such as the phase and amplitude of sinusoidal signals to variations in aquifer conductivity (K or T) and storage (S_s or S or S_y) parameters. The sensitivity maps produced through this analysis show that different frequencies of stimulation have different spatially distributed sensitivities to aquifer parameters. In particular, high-frequency oscillations tend to be more sensitive to parameters in the "near field," whereas low-frequency oscillations produce sensitivity maps that are more diffuse throughout the modeling domain. The steady-state response of aquifer head to a constant-rate pumping test is the extreme case of this with the most diffuse sensitivity, representing the zero-frequency limit of oscillatory testing.

[70] To demonstrate the use of multifrequency oscillatory aquifer stimulations in imaging, we presented a sample synthetic imaging problem. In this problem, a single testing arrangement was used, and the only parameter that was varied between individual aquifer tests was the frequency of the input stimulation. This test problem showed that progressive improvement in aquifer imaging results can be obtained by then jointly inverting multiple frequencies' responses. In the current analysis, we selected a few representative frequencies to invert (5, 10, 20, 100, 200, and 300 s), though inversion of many more frequencies may lead to even further improvement in imaging results.

7. Discussion and Future Work

[71] While the preliminary investigations in this work suggest that complementary information about heterogeneity can be obtained from multifrequency oscillatory hydraulic testing, we note that the tests performed in this work are not truly tomographic—i.e., we did not implement multiple source-receiver combinations. We believe that using data

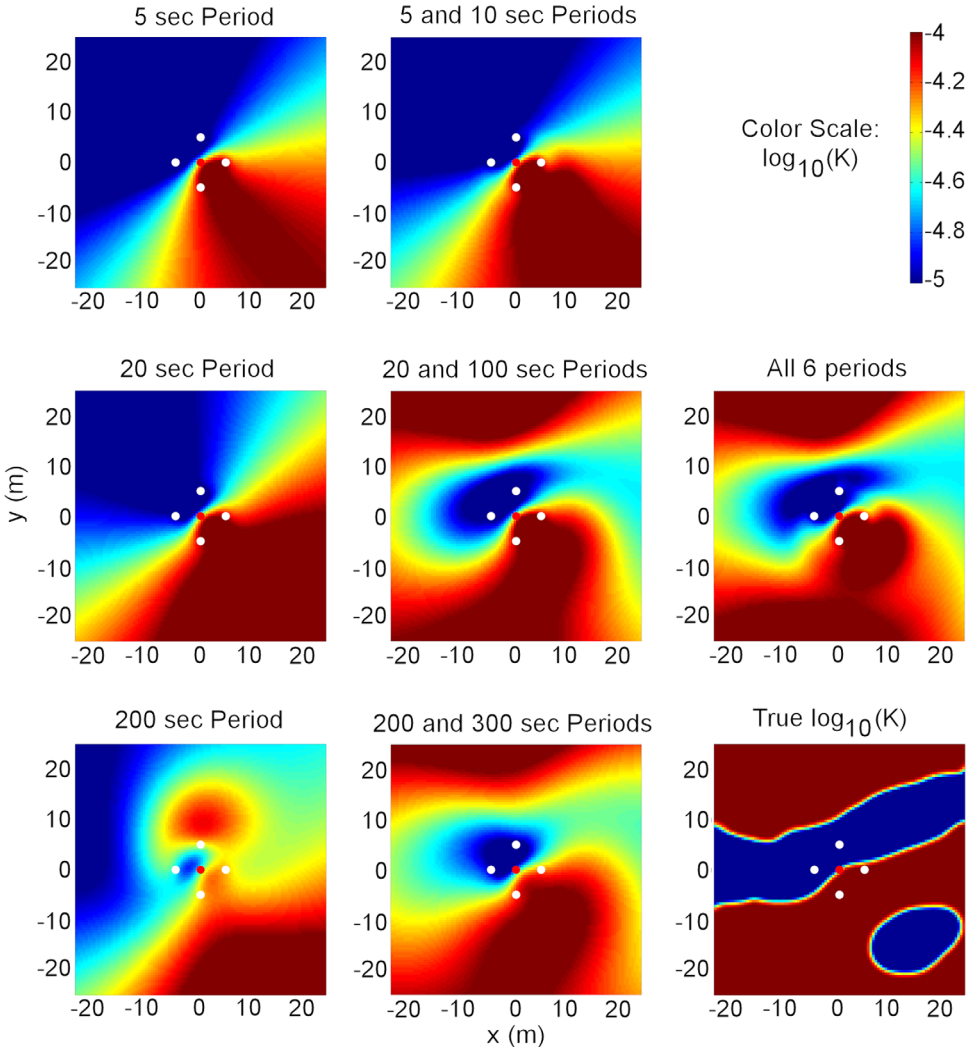

Figure 10. Comparison of inversion results obtained for representative single-frequency and multifrequency inversions. Area shown is the central 50 m × 50 m area of the synthetic model. First column shows single-frequency inversions. Second column shows two-frequency joint inversions. Third column shows six-frequency joint inversion (second panel), and true parameter field (third panel). Color scale is the same for all images.

Table 2. Root Mean Squared Error (RMSE) for Imaging Experiments[a]

Data Inverted	Central Area (50 m × 50 m)	Full Domain (150 m × 150 m)
5 s period	0.7653	0.8461
10 s period	0.7187	0.7614
5 and 10 s	*0.7183*	*0.7865*
20 s period	0.6618	0.6456
100 s period	0.583	0.6122
20 and 100 s	*0.3552*	*0.3343*
200 s period	0.5804	0.6716
300 s period	0.5166	0.5398
200 and 300 s	*0.3726*	*0.3845*
All six periods	*0.3468*	*0.3669*

[a]"Central area" refers to the area imaged in Figure 10, "full domain" refers to complete model, and italics indicate multifrequency inversions. Note general decrease in imaging error as more periods are inverted, especially within the central 50 m × 50 m area of model.

from a broad frequency "sweep" of oscillatory tests, while also altering source and receiver locations, may provide improved resolution of both fine-scale and large-scale aquifer features. In particular, it will be valuable to compare, under scenarios of realistic measurement noise and uncertainty, the imaging capabilities of transient hydraulic tomography and steady-state hydraulic tomography against M-OHI implemented in a tomographic fashion.

[72] It may seem counter-intuitive that oscillatory pumping tests could provide better information about aquifer heterogeneity than constant-rate pumping tests—after all, any pumping test can be represented in the Fourier domain as a superposition of sinusoidal tests at various frequencies. Thus, in essence, the transient response to a constant-rate pumping test could already be considered as a multifrequency aquifer stimulation. However, we believe that by focusing testing at particular frequencies using the M-OHI concept presented herein, it becomes easier to extract the "signal" (a single, known input frequency) from other

undesirable signals, drifts, and noises. Constant-rate pumping tests, when performed in the field, are often contaminated by spurious signals that can be difficult to separate from the input (pumping) signal (see, e.g., the removal of evapotranspiration required in *Cardiff et al*. [2009]). While processing of constant-rate pumping tests using a frequency-domain model could be performed, it may be difficult to accurately extract signal magnitudes at each frequency (due to the fact that all signals are simultaneously superposed), and likewise the ability to filter out noises is degraded.

[73] A key benefit of oscillatory signals, which has not been dealt with in much depth in this work, is the robustness of signal processing routines for extracting known-frequency oscillations from noisy data. In practice, we have found that even low-magnitude oscillating signals can often be accurately extracted from long-time series, i.e., a noisy, small-magnitude sinusoid measurement can be compensated for by obtaining a long enough record such that data errors (estimates of the signal amplitude and phase) are reduced over time (Bakhos et al., in review, 2013). Thus, even if it initially appears that no signal is observable at a large distance from an oscillating source, that signal may eventually become clear as a long data history is recorded. Such a prospect holds exciting implications for long-term aquifer monitoring, and for extending the effective spatial range of aquifer investigations. In most hydrologic investigations, longer periods of observation present greater modeling difficulties, since unknown effects from industrial supply wells, irrigation, rainfall, and so on, may become prominent and should be modeled. In contrast, oscillatory signals can be separated from other influences, and may represent the one case in which data effectively gets less noisy and more reliable over time.

[74] Last, an obvious question—and one that continually confounds groundwater investigations—is whether larger scales of 1–10 km^2 can be effectively characterized for hydrologic property variability using any available hydrologic techniques. While we believe that it may often be difficult to produce practical equipment to manually generate oscillatory signals that travel to these scales, *natural* oscillations—including tides, periodic river stage fluctuations, evapotranspiration signals, etc.—may provide energy for signals with the high amplitude and low frequency necessary to characterize such large regions. The variety of cyclical natural processes that manifest on time scales of days to years may represent a vast, untapped data source for large-scale aquifer characterization, if long-term passive instrumentation for collecting observations are implemented. In addition, steady-periodic theory may be applicable to analyzing intermittent pumping from water supply wells over seasonal or longer time scales.

[75] **Acknowledgments.** The authors would like to acknowledge the insightful and helpful comments of three anonymous reviewers, whose input improved this manuscript. This work was funded by NSF grants EAR-1215746, 1215742, and 1215768, "Collaborative Research: Fundamental Research on Oscillatory Flow in Hydrogeology" and by NSF grants EAR-0934680 and 0934596, "CMG Collaborative Research: Subsurface Imaging and Uncertainty Quantification."

References

Anderson, M., and J. McCray (2011), Foreword: Lessons learned about contaminant hydrogeology from legacy research sites, *Ground Water*, *49*, 617–619.

Bear, J. (1972), *Dynamics of Fluids in Porous Media*, Elsevier, New York.

Becker, M., and E. Guiltinan (2010), Cross-hole periodic hydraulic testing of inter-well connectivity, in Stanford Geothermal Workshop, SGP-TR-188, Stanford University, Stanford, CA, USA.

Berg, S., and W. Illman (2011), Three-dimensional transient hydraulic tomography in a highly heterogeneous glaciofluvial aquifer-aquitard system, *Water Resour. Res.*, *47*, W10507, doi:10.1029/2011WR010616.

Bernabe, Y., U. Mok, and B. Evans (2005), A note on the oscillating flow method for measuring rock permeability, *Intl. J. Rock Mech. Min. Sci.*, *43*, 311–316.

Black, J. H., and K. L. Kipp (1981), Determination of hydrogeological parameters using sinusoidal pressure tests: A theoretical appraisal, *Water Resour. Res.*, *17*, 686–692.

Bohling, G. C., X. Zhan, J. J. Butler, Jr., and L. Zheng (2002), Steady shape analysis of tomographic pumping tests for characterization of aquifer heterogeneities, *Water Resour. Res.*, *38*(12), 1324, doi:10.1029/2001WR001,176.

Bohling, G. C., J. J. Butler, Jr., X. Zhan, and M. D. Knoll (2007), A field assessment of the value of steady shape hydraulic tomography for characterization of aquifer heterogeneities, *Water Resour. Res.*, *43*, W05430, doi:10.1029/2006WR004932.

Bouwer, H., and R. Rice (1976), A slug test for determining hydraulic conductivity of unconfined aquifers with completely or partially penetrating wells, *Water Resour. Res.*, *12*, 423–428.

Brauchler, R., R. Liedl, and P. Dietrich (2003), A travel time based hydraulic tomographic approach, *Water Resour. Res.*, *39*(12), 1370, doi:10.1029/2003WR002262.

Brauchler, R., J.-T. Cheng, P. Dietrich, M. Everett, B. Johnson, R. Liedl, and M. Sauter (2007), An inversion strategy for hydraulic tomography: Coupling travel time and amplitude inversion, *J. Hydrol.*, *345*, 184–198.

Brauchler, R., R. Hu, P. Dietrich, and M. Sauter (2011), A field assessment of high-resolution aquifer characterization based on hydraulic travel time and hydraulic attenuation tomography, *Water Resour. Res.*, *47*, W03503, doi:10.1029/2010WR009635.

Butler, J. J., Jr. (1998), *The Design, Performance, and Analysis of Slug Tests*, Lewis, Boca Raton.

Butler, J. J., Jr., J. M. Healey, G. W. McCall, E. J. Garnett, and S. P. Loheide II (2002), Hydraulic tests with direct push equipment, *Ground Water*, *40*, 25–36.

Cardiff, M., and W. Barrash (2011), 3-D transient hydraulic tomography in unconfined aquifers with fast drainage response, *Water Resour. Res.*, *47*, W12518, doi:10.1029/2010WR010367.

Cardiff, M., and P. Kitanidis (2008), Efficient solution of nonlinear, underdetermined inverse problems with a generalized pde model, *Comput. Geosci.*, *34*, 1480–1491.

Cardiff, M., W. Barrash, P. Kitanidis, B. Malama, A. Revil, S. Straface, and E. Rizzo (2009), A potential-based inversion of unconfined steady-state hydraulic tomography, *Ground Water*, *47*, 259–270.

Cardiff, M., W. Barrash, B. Malama, and M. Thoma (2011), Information content of slug tests for estimating hydraulic properties in realistic, high-conductivity aquifer scenarios, *J. Hydrol.*, *403*, 66–82.

Cardiff, M., W. Barrash, and P. K. Kitanidis (2012), A field proof-of-concept of aquifer imaging using 3d transient hydraulic tomography with temporarily-emplaced equipment, *Water Resour. Res.*, *48*, W05531, doi:10.1029/2011WR011704.

COMSOL AB (2011), COMSOL Multiphysics User's Guide, version 4.2a ed, Sweden.

Dietrich, P., and C. Leven (2009), Direct push technologies, in *Groundwater Geophysics*, edited by R. Kirsch, chap. 12, pp. 347–366, Springer, Berlin.

Hess, A. E. (1986), Identifying hydraulically conductive fractures with a slow-velocity borehole flowmeter, *Can. Geotech. J.*, *23*, 69–78, doi:10.1139/t86-008.

Hess, K. (1989), Use of a borehole flowmeter to determine spatial heterogeneity of hydraulic conductivity and macrodispersion in a sand and gravel aquifer, Cape Cod, Massachusetts, in Proceedings of the Conference on New Field Techniques for Quantizing the Physical and Chemical Properties of Heterogeneous Aquifers, pp. 497–508, Natl. Water Well Assoc.

Hollaender, F., P. Hammond, and A. Gringarten (2002), Harmonic testing for continuous well and reservoir monitoring, paper SPE 77692 presented at the SPE Annual Technical Conference and Exhibition, Soc. of Pet. Eng., San Antonio, Tex.

Huang, S.-Y., J.-C. Wen, T.-C. J. Yeh, W. Lu, H.-L. Juan, C.-M. Tseng, J.-H. Lee, and K.-C. Chang (2011), Robustness of joint interpretation of

sequential pumping tests: Numerical and field experiments, *Water Resour. Res.*, *47*, W10530, doi:10.1029/2011WR010698.

Illman, W., X. Liu, and A. Craig (2007), Steady-state hydraulic tomography in a laboratory aquifer with deterministic heterogeneity: Multi-method and multiscale validation of hydraulic conductivity tomograms, *J. Hydrol.*, *341*, 222–234.

Illman, W. A., and P. J. Alvarez (2009), Performance assessment of bioremediation and natural attenuation, *Crit. Rev. Environ. Sci. Technol.*, *39*, 209–270.

Kabala, Z. J. (1993), The dipole flow test: A new single-borehole test for aquifer characterization, *Water Resour. Res.*, *29*, 99–107.

Kitanidis, P. K. (1995), Quasi-linear geostatistical theory for inversing, *Water Resour. Res.*, *31*, 2411–2419.

Kuo, C. (1972), Determination of reservoir properties from sinusoidal and multirate flow test in one or more wells, *SPE J.*, *12*, 499–507.

Leven, C., and P. Dietrich (2006), What information can we get from pumping tests? Comparing pumping test configurations using sensitivity coefficients, *J. Hydrol.*, *319*, 199–215.

Li, W., W. Nowak, and O. A. Cirpka (2005), Geostatistical inverse modeling of transient pumping tests using temporal moments of drawdown, *Water Resour. Res.*, *41*, W08403, doi:10.1029/2004WR003874.

Liu, X., W. Illman, A. Craig, J. Zhu, and T.-C. J. Yeh (2007), Laboratory sandbox validation of transient hydraulic tomography, *Water Resour. Res.*, *43*, W05404, doi:10.1029/2006WR005144.

Maineult, A., E. Strobach, and J. Renner (2008), Self-potential signals induced by periodic pumping tests, *J. Geophys. Res.*, *113*, B01203, doi:10.1029/2007JB005193.

McElwee, C. D., B. R. Engard, B. J. Wachter, S. A. Lyle, J. Healey, and J. F. Devlin (2011), *Hydraulic tomography and high-resolution slug testing to determine hydraulic conductivity distributions*, Kansas Geol. Surv. Open File Rep., p. 168. [Available at http://www.kgs.ku.edu/Hydro/Publications/2011/OFR11_2/index.html.]

Molz, F., G. Boman, S. Young, and W. Waldrop (1994), Borehole flowmeters: Field application and data analysis, *J. Hydrol.*, *163*, 347–371.

Neuman, S. P. (1972), Theory of flow in unconfined aquifers considering delayed response of the water table, *Water Resour. Res.*, *8*, 1031–1045.

Oliver, D. (1993), The influence of nonuniform transmissivity and storativity on drawdown, *Water Resour. Res.*, *29*, 169–178.

Paillet, F. L. (1998), Flow modeling and permeability estimation using borehole flow logs in heterogeneous fractured formations, *Water Resour. Res.*, *34*, 997–1010.

Rasmussen, T. C., K. G. Haborak, and M. H. Young (2003), Estimating aquifer hydraulic properties using sinusoidal pumping at the Savannah River Site, South Carolina, USA, *Hydrogeol. J.*, *11*, 466–482.

Renner, J., and M. Messar (2006), Periodic pumping tests, *Geophys. J. Intl.*, *167*, 479–493.

Rubin, Y., and S. S. Hubbard (Eds.) (2005), Hydrogeophysics, in *Water Science and Technology Library*, vol. *50*, Springer, the Netherlands.

Straface, S., T.-C. J. Yeh, J. Zhu, S. Troisi, and C. H. Lee (2007), Sequential aquifer tests at a well field, Montalto Uffugo Scalo, Italy, *Water Resour. Res.*, *43*, W07432, doi:10.1029/2006WR005287.

Townley, L. R. (1993), Aquifem-p: A periodic finite element aquifer flow model: User's manual and description, *Tech. Memo. 93/13*, 72 pp., CSIRO Div. of Water Resour, Australia.

Townley, L. R., and J. L. Wilson (1985), Computationally efficient algorithms for parameter estimation and uncertainty propagation in numerical models of groundwater flow, *Water Resour. Res.*, *21*, 1851–1860.

Vasco, D. (2008), Zeroth-order inversion of transient pressure observations, *Inverse Probl.*, *24*, 025013, doi:10.1088/0266-5611/24/2/025013.

Vasco, D., and S. Finsterle (2004), Numerical trajectory calculations for the efficient inversion of transient flow and tracer observations, *Water Resour. Res.*, *40*, W01507, doi:10.1029/2003WR002362.

Vasco, D., and K. Karasaki (2001), Inversion of pressure observations: An integral formulation, *J. Hydrol.*, *253*, 27–40.

Vasco, D., and K. Karasaki (2006), Interpretation and inversion of low-frequency head observations, *Water Resour. Res.*, *42*, W05408, doi:10.1029/2005WR004445.

Vasco, D., H. Keers, and K. Karasaki (2000), Estimation of reservoir properties using transient pressure data: An asymptotic approach, *Water Resour. Res.*, *36*, 3447–3465.

Vela, S., and R. McKinley (1970), How areal heterogeneities affect pulse-test results, *SPE J.*, *10*, 479–493.

Wu, C.-M., T.-C. J. Yeh, J. Zhu, T. H. Lee, N.-S. Hsu, C.-H. Chen, and A. F. Sancho (2005), Traditional analysis of aquifer tests: Comparing apples to oranges?, *Water Resour. Res.*, *41*, W09402, doi:10.1029/2004WR003717.

Yeh, J. T.-C., and S. Liu (2000), Hydraulic tomography: Development of a new aquifer test method, *Water Resour. Res.*, *36*, 2095–2105.

Yin, D., and W. Illman (2009), Hydraulic tomography using temporal moments of drawdown recovery data: A laboratory sandbox study, *Water Resour. Res.*, *45*, W01502, doi:10.1029/2007WR006623.

Zhu, J., and J. T.-C. Yeh (2005), Characterization of aquifer heterogeneity using transient hydraulic tomography, *Water Resour. Res.*, *41*, W07028, doi:10.1029/2004WR003,790.

Zhu, J., and T.-C. J. Yeh (2006), Analysis of hydraulic tomography using temporal moments of drawdown recovery data, *Water Resour. Res.*, *42*, W02403, doi:10.1029/2005WR004309.

Zlotnik, V., and B. Zurbuchen (1998), Dipole probe: Design and field applications of a single borehole device for measurements of vertical variations of hydraulic conductivity, *Ground Water*, *36*, 884–893.

Zlotnik, V. A., and V. L. McGuire (1998), Multi-level slug tests in highly permeable formations: 1. Modification of the Springer-Gelhar (SG) model, *J. Hydrol.*, *204*, 271–282.